CrystEngComm

PAPER

View Article Online
View Journal | View Issue

Check for updates

Cite this: *CrystEngComm*, 2023, **25**, 866

Revealing the supramolecular features of two Zn(II) complexes derived from a new hydrazone ligand: a combined crystallographic, theoretical and antibacterial study†

Samit Pramanik,[a] Anowar Hossain,[a] Sudipta Pathak, *[b] Sougata Ghosh Chowdhury,[c] Parimal Karmakar, [c] Antonio Frontera *[d] and Subrata Mukhopadhyay[a]

Received 20th October 2022,
Accepted 19th December 2022

DOI: 10.1039/d2ce01445a

rsc.li/crystengcomm

A new hydrazone ligand, HL [(1-methylimidazol-2-yl)methylene]isonicotinohydrazide, has been synthesized and characterized by several spectroscopic methods. The ligand (HL) was then utilized for the preparation of two new complexes, namely, $[Zn(L)_2]\cdot 2H_2O$ (complex **1**) and $[Zn(H_2L)Cl_3]\cdot H_2O$ (complex **2**). The crystal structures of these complexes have been established by single-crystal X-ray analysis. The non-covalent interactions and supramolecular assemblies observed in the crystal packing of both complexes have been described focusing on π···π (for **1**) and O···π–hole (for **2**) interactions along with various hydrogen bonding interactions. A DFT study has been carried out to analyse their non-covalent interactions with rationalization using molecular electrostatic potential (MEP) surfaces and the combined QTAIM/NCI plot computational tools. In addition, the *in vitro* biological activities of the synthesized ligand (HL) and the water-soluble complex **2** were evaluated against *Escherichia coli* and *Staphylococcus aureus*.

Published on 19 December 2022. Downloaded by Jadavpur University on 5/18/2023 8:47:12 AM.

Introduction

The field of non-covalent interactions (NCIs) is extensive and covers the whole of science. The NCIs involving hydrogen bonding, halogen bonding, π···π stacking, lone pair···π, cation···π, anion···π, C–H···π, N–H···π, and O–H···π interactions have attracted recent interest to elucidate the outstanding importance of these weak forces in controlling the structure and function of macromolecules.[1–7] A deep understanding of these weak interactions is essential to go forward in many fields, especially in crystal growth and crystal engineering.[8] Recently, much attention has also been given to π–hole interactions owing to their cooperative participation in chemical reactions and crystal engineering, as well as in biological applications. Theoreticians have established that the electron density distribution around covalently bonded atoms is not isotropic, *i.e.*, the atoms develop some regions of higher and lower electron density.[9] A π–hole can be defined as positive electrostatic potential on unoccupied π* orbitals, which have the capability to interact with some electron-dense region (anion, Lewis base, π-system, *etc.*).[10,11] It is typically located above and below to the molecular framework of π-systems, such as carbonyls or conjugated π–acidic systems, such as hexafluorobenzene.[12] One of the promising but comparatively less studied systems is the imidic C=N group, acting as a Lewis acid (π–hole donor).[13–15]

Schiff base ligands with nitrogen or oxygen donor atoms are a good class of organic compounds that play an important role by serving as chelating ligands in the main groups and transition metal coordination chemistry.[16,17] The diverse role of the transition metal complexes of Schiff base ligands in inorganic and metal–organic compounds and biochemistry has received considerable attention owing to their stability in different oxidative and reductive conditions.[18,19] Hydrazone ligands are a special type of Schiff base which can accommodate with different coordination modes according to the demand of variable geometries and valences of metal ions in coordination complexes.[20] Due to the presence of the N–H functionality adjacent to the azomethine (C=N) chromophore, they can form interesting hydrogen bonded self-assembly in metal complexes.[21]

[a] *Department of Chemistry, Jadavpur University, Kolkata 700032, India*
[b] *Department of Chemistry, Haldia Government College, Debhog, Purba Medinipur, 721657, West Bengal, India. E-mail: sudiptachemster@gmail.com*
[c] *Department of Life Science and Biotechnology, Jadavpur University, Kolkata 700032, India*
[d] *Departament de Química, Universitat de les Illes Balears, Crta. de Valldemossa km 7.5, 07122 Palma de Mallorca, Baleares, Spain. E-mail: toni.frontera@uib.es*

† Electronic supplementary information (ESI) available: Experimental details. CCDC 2209945 and 2209946. For ESI and crystallographic data in CIF or other electronic format see DOI: https://doi.org/10.1039/d2ce01445a

This journal is © The Royal Society of Chemistry 2023

Published on 19 December 2022. Downloaded by Jadavpur University on 5/18/2023 8:47:12 AM.

However, in the metal-coordinated hydrazone ligand, the electron withdrawing N–H group induces acidity to the imidic C=N bond which can interact with electron rich atoms and develop distinct supramolecular interaction.[22] The interaction of these donor ligands and metal ions gives complexes of different geometries, and a literature survey reveals that these complexes have biologically active properties such as anticancer, antifungal, antibacterial, anti-malarial, anti-inflammatory, antiviral, and antipyretic properties.[23–25] It should be noted that metal chelation can tremendously influence the antimicrobial/bioactive behavior of the organic ligands.[26] Thus, various transition metal complexes have been synthesized in this field.

After iron, zinc (Zn) is the second most abundant trace element in the human body and is one of the most important micro-elements for human physiology.[27] Zn^{2+} (d^{10} configuration) has zero ligand field stabilization energy that can support a variable coordination geometry around the metal centre (zinc) and assist the fast exchange of ligands.[28,29] Besides, due to the lack of redox activity of divalent zinc ions, this eliminates any chances of free radical reactions and makes it crucial for the body's antioxidant protection system.[27] However, a random mix of transition metal components such as Co–M (M = Zn, Cu, Fe) was reported in several studies to enhance the catalyst efficiency.[30] The importance of zinc in biological systems is related to its unique chemical properties. It plays an important role in the catalytic activity of various enzymes, protein synthesis, DNA synthesis, and immune functions and determines the conformations of many proteins through binding in the active sites. This makes zinc an essential element for all cellular functions and the development of all forms of life. Compared to other metal-based drugs, Zn(II) complexes generally exert lower toxicity and have fewer side effects.[31] In the last few years different classes of zinc coordination complexes have shown good potential in diverse applications, in nonlinear optics, in photo-catalysis and in several diseases, and as anti-inflammatory, anti-diabetic, antimicrobial, antioxidant, and antitumor agents.[32–40]

As a part of our efforts to explore the non-covalent interactions in coordination compounds, herein, we have designed and prepared two Zn(II) complexes (**1** and **2**) using a newly synthesized [(1-methylimidazol-2-yl)methylene] isonicotinohydrazide [**HL**] ligand in aqueous medium. Single crystal X-ray analysis shows that complex **1** is a distorted octahedron whereas complex **2** is a distorted tetrahedron in nature. Complex **1** shows π···π, O–H···π and hydrogen bonding interactions that are responsible for forming various supramolecular architectures. Interestingly, the non-coordinated water molecules are interconnected through hydrogen bonds to form a tetrameric water cluster which has a significant role in stabilizing the molecular structure of complex **1**. The solid-state structure of complex **2** is stabilized through $\pi\cdots\pi^+$ stacking, lone pair···π/π^+ and various types of hydrogen bonding interactions which are responsible for forming various supramolecular architectures. More importantly, the imidic C=N bond of the Zn(II)-coordinated hydrazone ligand is able to interact favorably with the electron-rich oxygen atom of a non-coordinated water molecule (O···π–hole interaction) in complex **2**, which is a rare example. Another interesting phenomenon is that the π-system of the –NNHCO– group takes part in the stacking interaction to give additional stability in complex **2**. These NCIs have been confirmed using combined QTAIM/NCI plot analysis and supported by MEP surface analysis. Moreover, the cooperative and energetic features of both conventional and unconventional interactions have also been evaluated by means of DFT calculations. In addition, the antibacterial activities of **HL** and its complex (**2**) were tested against Gram-negative (*Escherichia coli*) and Gram-positive (*Staphylococcus aureus*) bacteria.

Experimental

Materials and apparatus

All the chemicals (analytical grade) and solvents (spectroscopic grade) were purchased from commercial suppliers and used without any further purification. Freshly prepared double distilled water was used throughout the synthetic procedure, and all the reactions were carried out under aerobic conditions. Elemental analyses (C, H and N) were performed using a PerkinElmer 2400 Series-II CHN analyzer, a USA elemental analyzer. ESI mass spectra were obtained using a Water HRMS model XEVO-G2QTOF#YCA351 spectrometer. The ^{1}H NMR spectrum was obtained using a Bruker spectrometer (400 MHz) with DMSO-d_6 solvent using trimethylsilane (TMS) as an internal standard. Fourier transform infrared (FT-IR) spectra were recorded on a Perkin Elmer LX-1 FT-IR spectrophotometer (4000–400 cm^{-1}) by using a modern diamond attenuated total reflectance (ATR) accessory method. The single crystal structures were characterized using a single-crystal X-ray diffractometer (Bruker Smart Apex II).

Synthesis of [(1-methylimidazol-2-yl)methylene]isonicotinohydrazide [HL]

Isonicotinic hydrazide (0.137 g, 1 mmol) was added into 30 mL ethanolic solution of 1-methyl imidazole-2-carboxaldehyde (0.11 g, 1 mmol). The reaction mixture was then refluxed for 3 hours

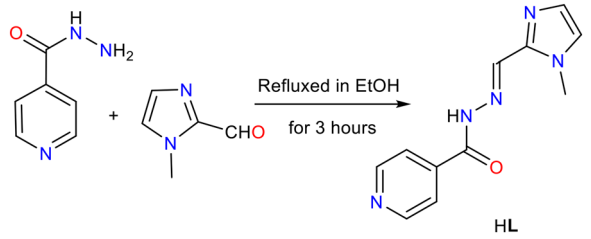

Scheme 1 Synthetic route for the ligand, HL.

Published on 19 December 2022. Downloaded by Jadavpur University on 5/18/2023 8:47:12 AM.

(Scheme 1). After completion of the reaction, the solution was cooled at room temperature. A light yellow solid formed, which was collected by filtration, washed repeatedly with cold water and dried in air. The desired product was obtained with good yield and acceptable purity. Yield 0.174 g (76%). The ligand (HL) is soluble in water ($S_{25°C} \approx 3.3$ mg mL^{-1}), methanol ($S_{25°C} \approx 4.2$ mg mL^{-1}), acetonitrile ($S_{25°C} \approx 3.8$ mg mL^{-1}) as well as in DMSO ($S_{25°C} \approx 5.1$ mg mL^{-1}). Anal. calc. for $C_{11}H_{12}N_5O$, C 57.63, H 4.84, N 30.55. Found: C 57.61, H 4.83, N 30.52%. ^{1}H NMR (400 MHz, $CDCl_3$): δ (ppm) = 12.11 (s, 1H), 8.78 (d, J = 6 Hz 2H), 8.42 (s, 1H), 7.81 (d, J = 6 Hz, 2H), 7.35 (d, J = 6 Hz, 2H), 7.08 (d, J = 7 Hz, 2H), 3.97 (s, 3H) (Fig. S1, ESI†). Main FT-IR absorptions, (KBr, cm^{-1}): 3210(bs), 3118(s), 3101(vs), 3054(s), 1683(s), 1456(vs), 1625(s), 1613(vs), 1602(s), 1556(s), 1525(s), 1499(s), 1471(s), 1437(s), 1412(s) (Fig. S2, ESI†). ESI-MS: m/z 252.150, 230.181; calcd. for [$C_{11}H_{12}N_5O$ + Na$^+$] = 252.089, [$C_{11}H_{12}N_5O$ + H$^+$] = 230.10 (Fig. S3, ESI†).

Synthesis of $[Zn(L)_2]\cdot 2H_2O$ (complex 1)

An aqueous suspension (20 mL) of the ligand, HL (0.229 g, 1 mmol), was added to 20 mL of aqueous $Zn(NO_3)_2\cdot 6H_2O$ (0.297 g, 1 mmol) solution with constant stirring (Scheme 2). A clear bright yellow solution was appeared after 3 hours of constant stirring. Then the solution was filtered, and the filtrate was left for slow evaporation without any disturbance. After one week, yellow coloured X-ray quality crystals of **1** were isolated (yield: 65%). Complex **1** is sparingly soluble in water ($S_{25°C} \approx 0.5$ mg mL^{-1}), slightly soluble in methanol ($S_{25°C} \approx 1.3$ mg mL^{-1}) and acetonitrile ($S_{25°C} \approx 0.9$ mg mL^{-1}), and completely soluble in DMSO ($S_{25°C} \approx 5.3$ mg mL^{-1}). Anal. calc. for $C_{11}H_{14}N_5O_3Zn$: C, 40.08; H, 4.28; N, 21.25. Found: C, 40.05; H, 4.26; N, 21.21%. Main FT-IR absorptions, (KBr, cm^{-1}): 3564(w), 3359(w), 3118(vs), 3098(vs), 3045(s), 2955(s), 1946(s), 1791(s), 1704(s), 1634(vs), 1604(s), 1595(s), 1565(vs), 1500(s), 1489(s), 1469(s), 1456(s), 1415(vs) (Fig. S4, ESI†).

Synthesis of $[Zn(H_2L)Cl_3]\cdot H_2O$ (complex 2)

Complex **2** was synthesised by reacting an aqueous suspension (20 mL) of the ligand, HL (0.229 g, 1 mmol) with 20 mL aqueous $ZnCl_2$ (0.136 g, 1 mmol) solution under stirring. The solution became turbid after one hour of constant stirring (Scheme 2). Two drops of 1 (M) HCl were added into the resultant turbid solution to obtain a clear pale yellow solution. Then the solution was filtered, and the filtrate was left undisturbed for slow evaporation. Two weeks later, deep yellow X-ray quality crystals of **2** were obtained (yield: 68%). Complex **2** is soluble in water ($S_{25°C} \approx 5.7$ mg mL^{-1}), methanol ($S_{25°C} \approx 3.7$ mg mL^{-1}), and acetonitrile ($S_{25°C} \approx 3.4$ mg mL^{-1}), as well as in DMSO ($S_{25°C} \approx 6.5$ mg mL^{-1}). Anal. calc. for $C_{11}H_{14}Cl_3N_5O_2Zn$: C, 31.46; H, 3.36; N, 16.67. Found: C, 31.44; H, 3.35; N, 16.64%. Main FT-IR absorptions, (KBr, cm^{-1}): 3507(s), 3402(s), 3200(s), 3144(vs), 3102(s), 3059(vs), 1979(s), 1673(vs), 1620(vs), 1544(vs), 1498(s), 1475(vs), 1422(vs) (Fig. S5, ESI†).

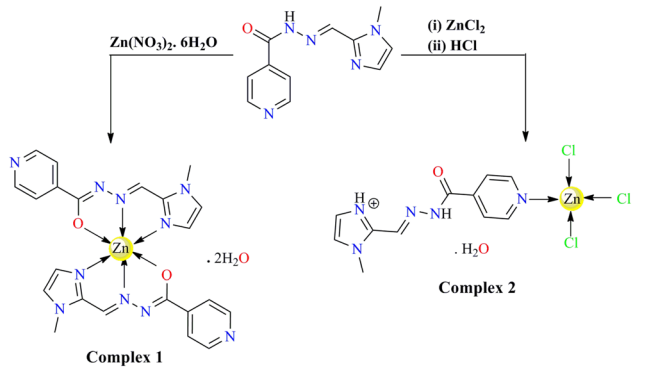

Scheme 2 Schematic representation of the synthesis of the title complexes.

X-ray crystallographic analysis

Single crystal X-ray data collections were made using a Bruker SMART APEX II CCD area detector equipped with a graphite monochromated Mo Kα radiation (λ = 0.71073 Å) source in the φ and ω scan modes at 296 K for both the complexes. Cell parameter refinement and data reduction for both complexes were carried out using a Bruker SMART APEX II instrument, Bruker SMART and Bruker SAINT software.[41] The crystal structures of the title compounds were solved by an intrinsic phasing method using SHELXT-2014/5 and refined by full-matrix least squares on F^2 techniques using the SHELXL-2016/6 crystallographic software package.[42] The CIFs have been deposited with CCDC no. 2209945 (complex **1**) and CCDC no. 2209946 (complex **2**). The selected crystal data for **1** and **2** are given in Table S1 (ESI†).

Theoretical methods

The calculations of the non-covalent interactions were carried out using Gaussian-16 (ref. 43) and the PBE0-D3/def2-TZVP level of theory[44,45] and the crystallographic coordinates. The interaction energies have been computed by calculating the difference between the energies of isolated monomers and their assembly. The interaction energies are corrected for the basis set superposition error (BSSE) employing the methodology proposed by Boys–Bernardi.[46] The Bader's "Atoms in molecules" theory (QTAIM)[47] has been used to study the interactions by means of the AIMAll calculation package.[48] The molecular electrostatic potential surfaces have been computed using the Gaussian-16 software and the 0.001 a.u. isovalue. To reveal the interactions in real space, we have used the NCIPLOT index[49] based on the reduced density gradient (RDG) isosurfaces that are derived from the electronic density and its first derivative. The sign of the second Hessian eigenvalue times the electron density [*i.e.* sign(λ_2)ρ in atomic units] enables the identification of attractive/stabilizing (blue-green coloured isosurfaces) or repulsive (yellow-red coloured isosurfaces) interactions using 3D-plots.[50]

 This journal is © The Royal Society of Chemistry 2023

Published on 19 December 2022. Downloaded by Jadavpur University on 5/18/2023 8:47:12 AM.

Bacterial strains and culture conditions

Properly distinguished cells of *E. coli DH5α* (K12) and *S. aureus* (ATCC 29737) were obtained from the National Institute of Cholera and Enteric Diseases (NICED), Kolkata, India. Cultures were nourished on Luria broth (LB). The bacteria were cultured overnight in 3 ml of LB in a shaker at 37 °C prior to incubation with complex **2**, ligand **HL**, and positive control $ZnCl_2$ until the absorbance of the culture reached 1.0 at 600 nm, indicating the colony formation of 10^9 CFU (colony-forming unit) ml^{-1}. Sterile broth was used to dilute the overnight cultures to 10^7 CFU ml^{-1}.

Antibacterial activity study

Complex **1** was sparingly soluble in water, whereas the ligand (**HL**) and complex **2** were completely soluble in water. Thus, we did not perform the antibacterial study for complex **1**. The antibacterial activity of $ZnCl_2$ and complex **2** was confirmed through the determination of minimum inhibitory concentration (MIC). The lowest concentration of the antimicrobial agent at which no growth is observed in medium is termed as MIC. 3 ml of LB was taken in test tubes, and each of them was inoculated with overnight cultures of the bacteria, and thereafter various concentrations of complex **2** (0–5 mM), ligand **HL** (0–5 mM) and $ZnCl_2$ (0–5 mM) were added in every test tube. The tubes were shaken at 37 °C for 24 h, and the absorbances were measured at 600 nm to determine bacterial growth.

Results and discussion

Synthesis

The facile condensation of isonicotinic hydrazide with 1-methyl imidazole-2-carboxaldehyde (1 : 1 molar ratio) in ethanol furnished a neutral *ONN* donor Schiff base ligand (**HL**), [(1-methylimidazol-2-yl)methylene]isonicotinohydrazide. After isolation and characterization by several spectroscopic techniques, the ligand (**HL**) was utilized to prepare two zinc(II) complexes, namely, $[Zn(\mathbf{L})_2]\cdot 2H_2O$ (**1**) and $[Zn(H_2\mathbf{L})Cl_3]\cdot H_2O$ (**2**). Complex **1** was produced by reacting the ligand (**HL**) with $Zn(NO_3)_2\cdot 6H_2O$ in an aqueous medium, whereas complex **2** was synthesized by treating $ZnCl_2$ with the ligand (**HL**) in the presence of dilute hydrochloric acid in water. In complex **1**, the ligand (**HL**) acts as an *ONN* tridentate chelating ligand, but in complex **2**, due to the protonation of the imidazole nitrogen atom, the chelating ability of the ligand (**HL**) was diminished, and it behaved as a simple monodentate ligand. Thus, a small variation in the reaction condition leads to the formation of zinc(II) complexes with two different geometries (distorted octahedra for **1** and distorted tetrahedra for **2**). The complexes were separated as block-shaped yellow single crystals from their mother solutions. The synthetic route for the complexes is shown in Scheme 2.

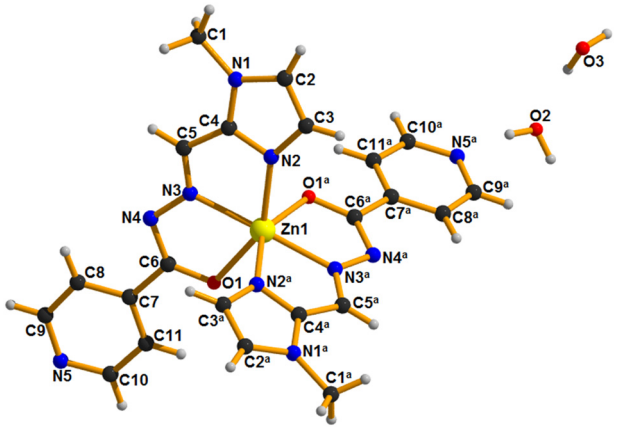

Fig. 1 Perspective view of complex **1**.

Structural description of complex 1

The perspective view of complex **1** with atom numbering scheme is displayed in Fig. 1. The single crystal X-ray diffraction study shows that the asymmetric unit of complex **1** consists of one-half of $[Zn(\mathbf{L})_2]$ unit (the other half being generated by an inversion center) and two non-coordinated water molecules.

Complex **1** crystallizes in a monoclinic system with the space group *C*2/*c*. The metal centric bond lengths and bond angles are summarized in Tables S2 and S3, respectively (ESI†). During complex formation, the ligand undergoes lactam–lactim tautomerism, and the deprotonation of the mono-negative ligand ($\mathbf{L}^-$) results in the formation of first order inner metallic complex. Here, the ligand acts as the *ONN* tridentate chelating ligand through O1, N3 and N2 atoms that occupy the respective meridional planes resulting in a distorted octahedral geometry around the Zn(II) ion. The great distortion from the regular octahedral geometry is mainly due to the formation of four planar 5-membered chelate rings having bite angles in the range from 72.42(6)° to 76.76(6)°. The average Zn–N and Zn–O bond distances are 2.1388 Å and 2.1877 Å, respectively, which are in the range found for similar kinds of octahedral Zn(II) complexes. The electrical charge on the metal centre is stabilized by the two deprotonated Schiff base ligands ($\mathbf{L}^-$).

Complex **1** is stabilized through π···π stacking, O–H···π and hydrogen bonding (C–H···O, O–H···N and O–H···O) interactions (Tables S4–S6†) that are responsible to form various supramolecular architectures. In complex **1**, the non-coordinated water molecules interact among themselves through two different self-complementary hydrogen bonding interactions (O3–H3A···O2 and O3–H3B···O2) to form a tetrameric water cluster having a $R_4^2(8)$ ring motif (Fig. 2). These water clusters connect the monomeric units of complex **1** by O2–H2A···N5 (169°) hydrogen bonding interactions to produce a 1D zigzag polymeric chain as depicted in Fig. 2.

Bulk water is assumed to be a combination of various small water clusters like dimers, trimers, tetramers,

Published on 19 December 2022. Downloaded by Jadavpur University on 5/18/2023 8:47:12 AM.

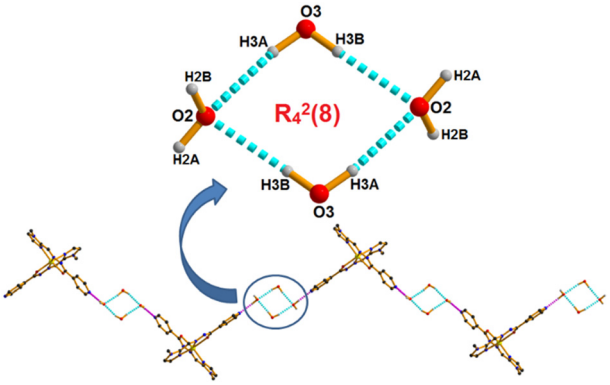

Fig. 2 Formation of 1D zigzag polymeric chain and the perspective view of water cluster through hydrogen bonding interactions in complex **1**.

pentamers, hexamers, *etc.*[51] Water clusters are smaller assemblies of a limited number of water molecules, and they are very interesting for analysis as they can reveal the nature of host–guest interactions at the molecular level.[52] Among the water clusters, the cyclic water tetramer is particularly interesting as it plays a vital role in understanding the two-structure model of liquid water and ice.[53] The study of the possible structures of water clusters in different surroundings is important to understand the nature of water–water interactions in the ice or bulk water, as well as in many biological and chemical processes.[54] Water tetramers encapsulated within different metal complex hosts have been reported by several researchers.[51,52,55–57] In our work, the water tetramer may be assigned to have a D_{2h} symmetry.

In another structure metallic moieties are connected through π···π interactions [Cg(5)···Cg(6)] and form dimeric structures, which are further connected through chelate ring···π interactions [Cg(1)···Cg(6) and Cg(3)···Cg(6)] and generate a 2D layered structure in *bc* plane as shown in Fig. 3. The interplanar spacing of Cg(5)···Cg(6), Cg(1)···Cg(6) and Cg(3)···Cg(6) is 3.8699(14) Å, 3.8699(14) Å and 3.8699(14) Å respectively.

Interestingly, the water cluster helps in the growth of the molecular crystal by filling the void spaces present in

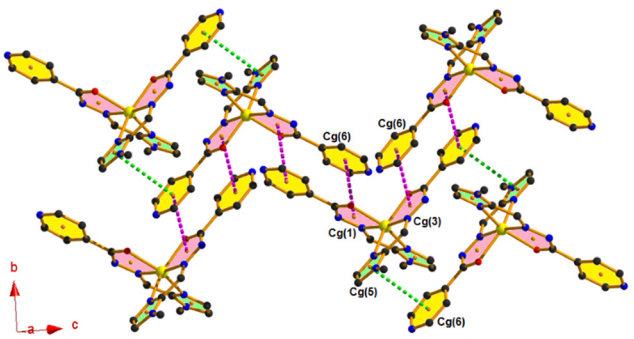

Fig. 3 Formation of supramolecular assembly through π···π interactions in complex **1**.

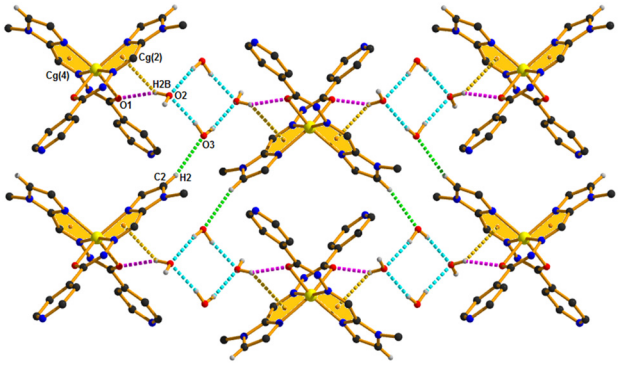

Fig. 4 Perspective view of the formation of a 2D architecture through O–H···π and hydrogen bonding interactions in complex **1**.

complex **1** through O2–H2B···O1 and O2–H2B···Cg(2) [O–H···π] hydrogen bonding interactions. Here, the hydrogen atom (H2B) of the water molecule interacts simultaneously with carbonyl oxygen (O1) and Cg(2) of the same monomeric unit in a bifurcated manner to produce a 1D chain.

Such parallel chains are further connected through weak C2–H2···O3 interactions symbiotically to generate a 2D architecture, as shown in Fig. 4. The space-filling model (Fig. S6†) reveals how the tetrameric water cluster helps in the growth of the molecular crystal by filling the void spaces present in complex **1**.

Structural description of complex 2

The perspective view of complex **2** with the atom numbering scheme is shown in Fig. 5. The asymmetric unit of complex **2** shows one [Zn(H$_2$**L**)Cl$_3$] unit and one non-coordinated water molecule. Structural investigation shows that the complex adopts a monoclinic crystal system with the $P2_1/c$ space group, and its unit cell comprises four asymmetric units. The metal centric bond lengths and bond angles are tabulated in Tables S2 and S3, respectively (ESI†). Protonation of the imidazole nitrogen atom (N2) inhibits the chelating ability of the Schiff base ligand (H**L**), and thus it behaves as a simple monodentate ligand instead of an *ONN* tridentate chelating ligand towards a Zn(II) ion. The Zn(II) ion is in a distorted tetrahedral environment completed by one pyridine nitrogen

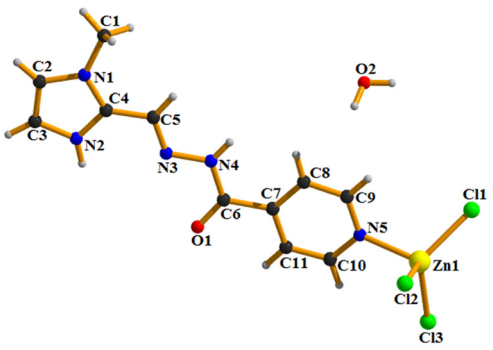

Fig. 5 Perspective view of complex **2**.

This journal is © The Royal Society of Chemistry 2023

Published on 19 December 2022. Downloaded by Jadavpur University on 5/18/2023 8:47:12 AM.

atom (N5) of the protonated Schiff base ligand (H_2L^+) and three chloride anions (Cl1, Cl2 and Cl3). The degree of distortion of the Zn(II) ion can be expressed using the parameter τ_4 (τ_4 = 0.88; τ_4 = 0 for a square planar geometry and τ_4 = 1 for a tetrahedral geometry).[58]

The bond angles around the metal center are ranging from 101.88(6)° to 119.21(3)° indicating the deviation from the ideal tetrahedral geometry. The overall tripositive charge of the complex is satisfied by the three chloride ions.

The solid-state structure of complex **2** is stabilized through π···π stacking, lone pair···π and various types of hydrogen bonding (C–H···Cl, N–H···O, N–H···Cl, O–H···N, O–H···O and O–H···Cl) interactions (Tables S4–S6†). The self-complementary nature of complex **2** results in a 2D architecture involving π···π^+ and lone pair···π^+ interactions (Fig. 6). Here, the oxygen atom (O1) of the carbonyl group (attached with one complex unit) interacts with Cg(1) of the adjacent protonated imidazole ring (π^+), which in turn interacts with Cg(2) of another unit having an interplanar spacing of 3.710(2) Å. Hence the combined effect of the lone pair···π^+ and π···π^+ interactions mutually strengthens each other.

A different 2D supramolecular network is generated incorporating lone pair···π and hydrogen bonding interactions (Fig. 7). Here, the coordinated chlorine atom (Cl2) interacts with the complex unit through two different intermolecular hydrogen bonding (C5–H5···Cl2 and N4–H4C···Cl2) interactions that lead to the formation of an $R_2^1(6)$ ring motif. Now, these ring motifs are further connected through the self-complementary lone pair···π interactions where the lone pair of coordinated chlorine atom (Cl3) faces towards the Cg(2) ring of the adjacent unit at (1 − *x*, 2 − *y*, 1 − *z*) with an angle of 101.49(3)°. Thus the lone pair···π interactions along with these two types of intermolecular hydrogen bonding interactions enhance the dimensionality from 1D to 2D as shown in Fig. 7.

In complex **2**, the non-coordinated water molecule interacts with the complex unit by the three different

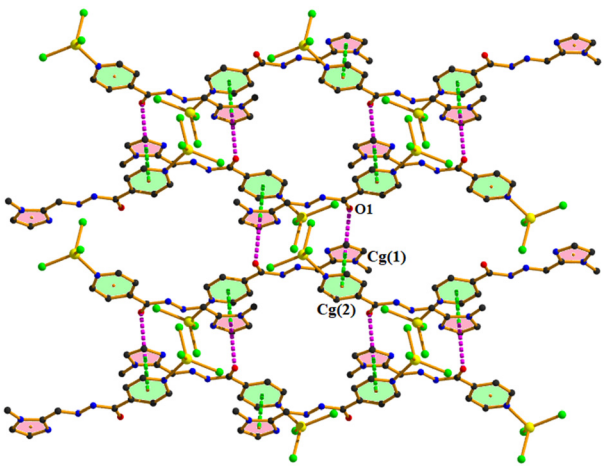

Fig. 6 Perspective view of the formation of a 2D architecture through π···π^+ stacking and lone pair···π^+ interactions in complex **2**.

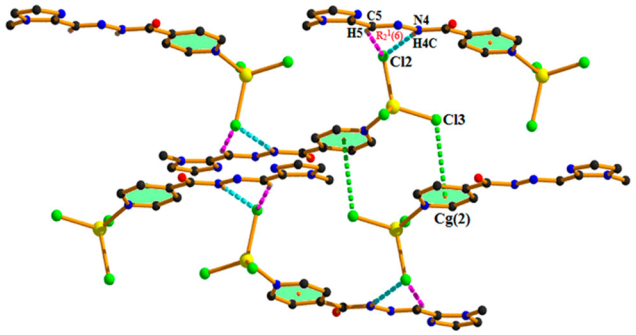

Fig. 7 Perspective view of the 2D supramolecular network through lone pair···π and hydrogen bonding interactions in complex **2**.

intermolecular hydrogen bonding (N2–H2C···O2, O2–H2A···N3, and O2–H2A···O1) interactions that lead to the formation of two different types of synthons, namely, $R_2^2(7)$ [A] and $R_1^2(5)$ [B]. These two synthons (A and B) are further connected by another type of intermolecular hydrogen bonding (O2–H2B···Cl3) interaction to form a 1D zigzag polymeric chain (Fig. 8). Now, the adjacent chains interact themselves through unconventional O2···C5 contact (tetrel bond) in a self-complementary manner resulting in a 2D layered assembly in the *bc*-plane (Fig. 8). Here, the oxygen atom (O2) of water molecule is also close to the carbon atom (C5) of the C=N bond, *i.e.*, 3.132 Å (shorter than the sum of their van der Waals radii 3.22 Å),[59] which indicates a significant O···π–hole interaction.

Protonation of the nitrogen atom (N2) of the imidazole ring enhances the positive potential over the C=N bond favoring the π–hole interaction with an electron rich oxygen atom (O2), which is strongly supported by the MEP surface analysis, as well as by the QTAIM/NCI plot in the theoretical part.

DFT calculations

The theoretical study is devoted to the analysis of the hydrogen bonds involving the co-crystallized water molecules, both in the water cluster and between the water and the ligands.

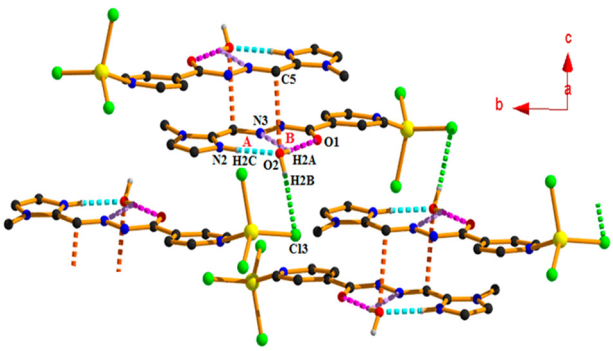

Fig. 8 2D layered assembly through O···π–hole and hydrogen bonding interactions in complex **2**.

Published on 19 December 2022. Downloaded by Jadavpur University on 5/18/2023 8:47:12 AM.

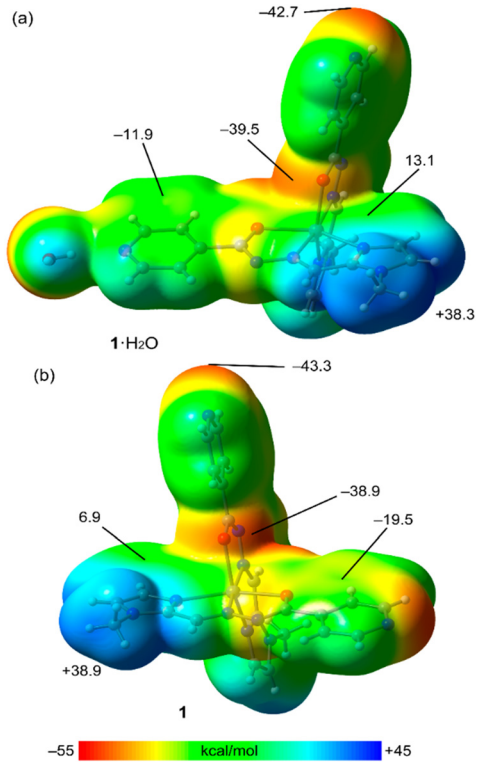

Fig. 9 MEP surface of complexes $1{\cdot}H_2O$ (a) and **1** (b). Isovalue 0.001 a.u. The energies at the selected points of the surfaces are given in kcal mol^{-1}. Level of theory: PBE0-D3/def2-TZVP.

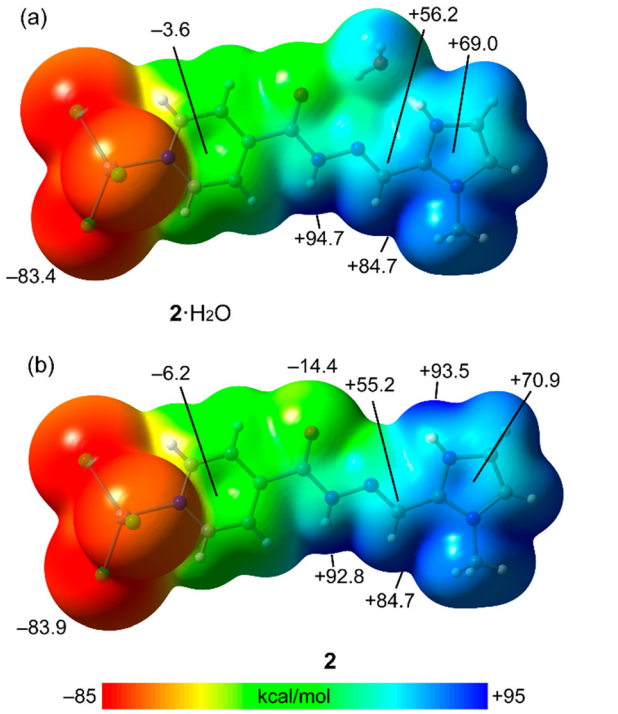

Fig. 10 MEP surface of complexes $2{\cdot}H_2O$ (a) and **2** (b). Isovalue 0.001 a.u. The energies at the selected points of the surfaces are given in kcal mol^{-1}. Level of theory: PBE0-D3/def2-TZVP.

Moreover, we have also analysed the influence of the water molecules on the electronic structure of the ligands and their ability to form π-stacking interactions.

We have first computed the MEP surfaces of the complexes **1** and **2** with and without the hydrogen-bonded water molecules. The MEP surfaces of $1{\cdot}H_2O$ and **1** are represented in Fig. 9, evidencing that the MEP minimum is located at the pyridine N-atom followed by the coordinated O-atom of the hydrazide ligand. The hydrogen-bonded water molecule slightly affects the MEP values over the aromatic rings, making the MEP values more positive. That is, the MEP value over the pyridine ring changes from −19.5 kcal mol^{-1} in **1** to −11.9 kcal mol^{-1} in $1{\cdot}H_2O$, and that over the imidazole ring increases from 6.9 kcal mol^{-1} in **1** (Fig. 9b) to 13.1 kcal mol^{-1} in $1{\cdot}H_2O$. The different electronic natures of both rings support the formation of the π-stacking assemblies described in Fig. 3, where the pyridine ring is stacked over the imidazole ring, which is electrostatically favoured.

The MEP surfaces of $2{\cdot}H_2O$ and **2** are represented in Fig. 10, showing that the MEP minimum is located at the chlorido ligands of Zn^{2+}, as expected. The MEP maximum is located at the NH of the hydrazide group in $2{\cdot}H_2O$ and in the imidazole group in **2**. In this complex, the MEP over the imidazole ring is very large and positive due to its protonation. The MEP over this ring is only slightly reduced by the formation of the hydrogen bond with the water molecule.

The effect of the hydrogen-bonded water on the pyridine ring is also small, slightly changing the MEP value from −6.2 kcal mol^{-1} in **2** to −3.6 kcal mol^{-1} in $2{\cdot}H_2O$. Finally, it is worth mentioning that the MEP value over the C-atom of the C═N bond is large and positive (+56.2 kcal mol^{-1} in $2{\cdot}H_2O$), which is thus adequate for interaction with electron rich atoms, as further analysed below.

The strength of the different hydrogen bonds involving the water molecules has been studied using the QTAIM method for the water cluster in **1** and also for the $1{\cdot}H_2O$ and $2{\cdot}H_2O$ dimers. Each hydrogen-bond is characterized by a bond critical point CP (represented as a small red sphere) and a bond path (dashed bond) connecting the H-atoms to the O/N-atoms (see Fig. 11).

The energetic results are also indicated in Fig. 11, disclosing the strong nature of the O–H···N and N–H···O H-bonds in $1{\cdot}H_2O$ and $2{\cdot}H_2O$ dimers, respectively (−6.1 kcal mol^{-1} in **1** and −6.0 kcal mol^{-1} in **2**). The QTAIM analysis confirms the existence of the three hydrogen-bonds in the $2{\cdot}H_2O$ dimer connecting the water molecule to the ligand. Due to the worse directionality and longer distance, the O–H···N is the weakest one (Fig. 11c). The total interaction energy is very large (−12.2 kcal mol^{-1}) due to the contribution of the three hydrogen-bonds, fixing the position of the water molecule and explaining the co-crystallization. Regarding the water cluster of **1**, the individual O–H···O hydrogen-bonds are generally weaker than those observed between water and the ligands; however the binding energy is significant (−12.6 kcal mol^{-1}) and similar to those previously reported for this type of cluster.[60]

 This journal is © The Royal Society of Chemistry 2023

Published on 19 December 2022. Downloaded by Jadavpur University on 5/18/2023 8:47:12 AM.

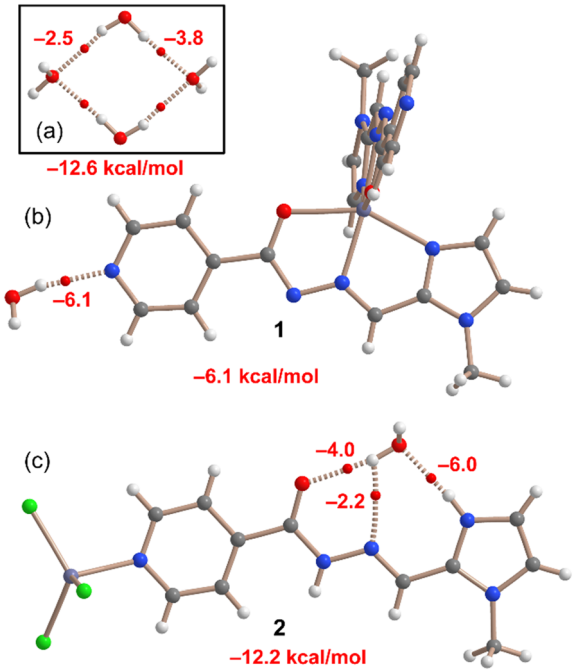

Fig. 11 QTAIM analysis (bond CPs in red) of the water cluster (a), **1**·H_2O dimer (b) and **2**·H_2O (c). The individual and total hydrogen-bond energies are indicated next to the bond CPs. Only intermolecular bond CPs and bond paths are presented.

We have also studied the influence of the water molecule on the π-stacked dimers observed in the solid state of **1**, which is described in Fig. 3. To do so, we have computed the binding energies of the dimers with and without the presence of the hydrogen-bonded water molecule, as indicated in Fig. 12. Moreover, the combined QTAIM/NCI plot analysis of the dimer is also included in Fig. 12. The NCI plot, *via* the representation of the reduced density gradient (RDG) isosurfaces, is very convenient to represent noncovalent interactions in real space. The QTAIM/NCI plot analysis confirms the existence of the pyridine···imidazole π-stacking interactions, characterized by two bond CPs, bond paths and extended green RDG isosurfaces. Moreover, the analysis also shows the participation of the chelate ring (CR) interactions, since two atoms of the five membered CRs are connected *via* two bond CPs, bond paths and green RDG isosurfaces. Other ancillary interactions are also observed like the C–H···π and C–H···N contacts, both characterized by the corresponding bond CPs, bond paths and green isosurfaces. This intricate combination of interactions explains the large interaction energy of this assembly (ΔE_1 = −23.6 kcal mol^{-1}) and confirms its relevance in the solid state of complex **1**. The binding energy without the presence of the hydrogen-bonded water molecules is only reduced to ΔE_2 = −22.7 kcal mol^{-1}, thus suggesting that the water molecule slightly reinforces the stacking, in line with the small differences observed in the MEP values over the aromatic rings (see Fig. 9).

A similar analysis has been performed for complex **2** (see Fig. 13), showing a different behaviour. That is, the binding energy of the π-stacked dimer is strongly influenced by the presence of the water molecule. This is due to the formation of an extra interaction (O···C) where the O-atom of the water molecule is located over the imidic C-atom, thus forming a O···π–hole contact. This is strongly supported by the QTAIM/NCI plot analysis, which shows a bond CP, bond path and green isosurface connecting the O and C-atoms. The difference between the dimerization energies (with and without water) is −6 kcal mol^{-1}, thus disclosing that such contacts are energetically significant and further contributes to the stabilization of the assembly. Moreover, the extended RDG isosurface located between the imidazole ring and the hydrazido group suggests that the π-system of the –NNHCO– groups participate in the stacking interaction.

Antibacterial effects of complex 2

Minimum inhibitory concentration affirms the antibacterial activity of complex **2** and positive control $ZnCl_2$ on both Gram-positive and Gram-negative bacteria as shown in Fig. 14. A lower concentration of complex **2** (1.89 mM) completely inhibits the growth of Gram-positive bacteria whereas a higher

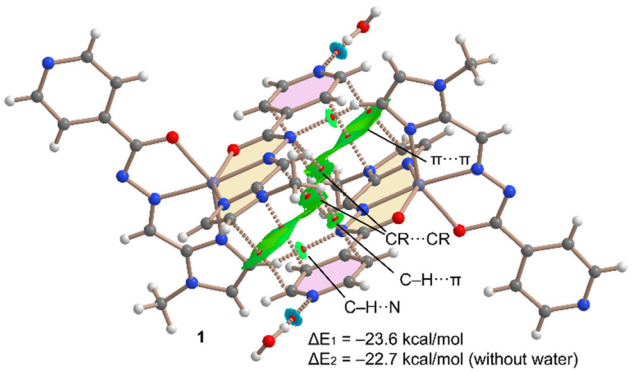

Fig. 12 QTAIM analysis of intermolecular bond CPs (red spheres) and bond paths (dashed lines) of **1**·H_2O. Only intermolecular interactions are shown. The settings for the NCIplot are as follows: RDG = 0.5, ρ cut-off = 0.04 a.u., color scale −0.04 a.u. ≤ sign(λ_2)ρ ≤ 0.04 a.u.

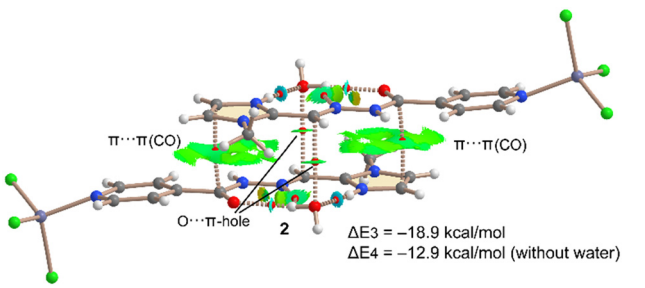

Fig. 13 QTAIM analysis of the intermolecular bond CPs (red spheres) and bond paths (dashed lines) of **2**·H_2O. Only intermolecular interactions are shown. The settings for the NCIplot are the following: RDG = 0.5, ρ cut-off = 0.04 a.u., color scale −0.04 a.u. ≤ sign(λ_2)ρ ≤ 0.04 a.u.

Published on 19 December 2022. Downloaded by Jadavpur University on 5/18/2023 8:47:12 AM.

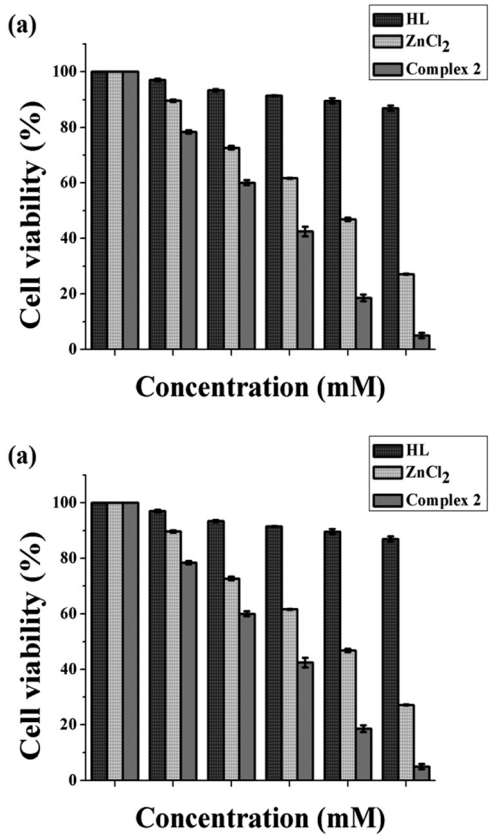

Fig. 14 Determination of minimum inhibitory concentration of ligand HL and complex **2** toward the (a) *E. coli DH5α* strain and (b) *S. aureus* strain. The results are the mean ± SD of two independent experiments.

concentration (2.64 mM) of the same was needed to inhibit the growth of Gram-negative bacteria. The MIC of $ZnCl_2$ required to inhibit the growth of *S. aureus* and *E. coli* was found to be 2.93 mM and 3.34 mM, respectively, indicating that complex **2** has higher antibacterial activity than $ZnCl_2$. However, ligand H**L** did not show any cytotoxic activity. The findings suggest that complex **2** has more antibacterial effect on the Gram-positive *S. aureus* strain than the Gram-negative *E. coli* strain due to the different natures of their cell walls. The cell walls of Gram-positive bacteria are composed of a thick peptidoglycan layer and teichoic acid, allowing various molecules including complex **2** to penetrate, unlike Gram-negative bacteria which inhibits the penetration of any external molecule due to presence of a unique protective outer membrane and a thin peptidoglycan layer in their cell wall.

The higher percentage in the bar graph indicates biocompatibility, whereas the lower percentage shows enhanced cell mortality. The decrease in the number of active bacterial cells on the treatment with complex **2** can be ascribed to lipophilicity and cell permeability.[61] The interaction between the Zn(II) ion and cell membrane through electrostatic forces destroys the plasma membrane and cause leakage of intracellular materials.[62]

Moreover, the protonation of the hydrazone ligand (H**L**) diminishes its chelation properties and makes complex **2** more polar, preferring stronger interactions with the amino acids/proteins in bacteria. Another concept is that the metal complex can hampers the process of respiration of cells, which lead to the blockage in the synthesis of proteins causing the death of bacteria.[63]

Conclusions

In conclusion, we have successfully synthesized two Zn(II) complexes (complexes **1** and **2**) using [(1-methylimidazol-2-yl) methylene]isonicotinohydrazide [H**L**] as the backbone ligand with two different metal salts and crystallographically characterized and explored the non-covalent interactions related with their crystal structures. The DFT study discloses the importance of the water lattice molecules in the solid state of complexes **1** and **2**. The energetic features of the hydrogen-bonds have been studied, either interacting with the hydrogen-bond donor and acceptor groups of the ligands or forming a tetrameric water cluster.

Moreover, the influence on the stacking assemblies of complexes **1** and **2** has been studied both energetically and using MEP surface analysis, showing a strong influence in **2** due to the formation of additional π–hole O···C tetrel bonds. The QTAIM analysis further confirms that the π-system of the –NNHCO– groups participate in the stacking interaction to give additional stability to complex **2**. Besides, complex **2** shows better antibacterial activity against the Gram-positive *S. aureus* (1.89 mM) over the Gram-negative *E. coli DH5α* (2.64 mM) bacteria, whereas the ligand (H**L**) exhibits no such activity.

Author contributions

Samit Pramanik, Anowar Hossain, and Sudipta Pathak: investigation, methodology, data analysis and general discussion. Antonio Frontera: DFT calculation and silico studies. Subrata Mukhopadhyay: conceptualization, supervision, and validation. Sougata Ghosh Chowdhury and Parimal Karmakar: biological application. All the authors have given approval to the final version of the manuscript.

Conflicts of interest

There are no conflicts to declare.

Acknowledgements

Samit Pramanik is thankful to the Council of Scientific and Industrial Research (CSIR, file no. 09/096(0947)/2018-EMR-I), New Delhi, for providing Senior Research Fellowship. We thank the MICIU/AEI from Spain for financial support (project number PID2020-115637GB-I00, FEDER funds).

References

1 K. T. Mahmudov, M. N. Kopylovich, M. F. C. Guedes da Silva and A. J. L. Pombeiro, *Coord. Chem. Rev.*, 2017, **354**, 54–72.

 This journal is © The Royal Society of Chemistry 2023

Published on 19 December 2022. Downloaded by Jadavpur University on 5/18/2023 8:47:12 AM.

2 I. A. Rather, S. A. Wagay and R. Ali, *Coord. Chem. Rev.*, 2020, **415**, 213327–213387.
3 (*a*) M. Mitra, P. Manna, A. Bauzá, P. Ballester, S. K. Seth, S. R. Choudhury, A. Frontera and S. Mukhopadhyay, *J. Phys. Chem. B*, 2014, **118**, 14713–14726; (*b*) A. Das, S. R. Choudhury, C. Estarellas, B. Dey, A. Frontera, J. Hemming, P. Gamez and S. Mukhopadhyay, *CrystEngComm*, 2011, **13**, 4519–4527; (*c*) A. Il'ya, D. Escudero, A. Frontera, P. V. Solntsev, E. B. Rusanov, A. N. Chernega, H. Krautscheid and K. V. Domasevitch, *Dalton Trans.*, 2009, 2856–2864.
4 K. T. Mahmudov, A. V. Gurbanov, F. I. Guseinov and M. F. C. Guedes da Silva, *Coord. Chem. Rev.*, 2019, **387**, 32–46.
5 S. Jena, J. Dutta, K. D. Tulsiyan, A. K. Sahu, S. S. Choudhury and H. S. Biswal, *Chem. Soc. Rev.*, 2022, **51**, 4261–4286.
6 (*a*) S. Pramanik, S. Pathak, S. Jana, M. Mondol, A. Frontera and S. Mukhopadhyay, *New J. Chem.*, 2021, **45**, 12108–12119; (*b*) L. A. Barrios, G. Aromi, A. Frontera, D. Quinonero, P. M. Deya, P. Gamez, O. Roubeau, E. J. Shotton and S. J. Teat, *Inorg. Chem.*, 2008, **47**, 5873–5881; (*c*) C. Garau, D. Quiñonero, A. Frontera, P. Ballester, A. Costa and P. M. Deyà, *Org. Lett.*, 2003, **5**, 2227–2229.
7 N. Mohan, K. P. Vijayalakshmi, N. Koga and C. H. Suresh, *J. Comput. Chem.*, 2010, **31**, 2874–2882.
8 G. R. Desiraju, *J. Am. Chem. Soc.*, 2013, **135**, 9952–9967.
9 P. Politzer, J. S. Murray and T. Clark, *Phys. Chem. Chem. Phys.*, 2013, **15**, 11178–11189.
10 D. Dutta, P. Sharma, A. Frontera, A. Gogoi, A. K. Verma, D. Dutta, B. Sarma and M. K. Bhattacharyya, *New J. Chem.*, 2020, **44**, 20021–20038.
11 P. Politzer, J. S. Murray and T. Clark, *J. Phys. Chem. A*, 2019, **123**, 10123–10130.
12 A. Bauzá, A. V. Sharko, G. A. Senchyk, E. B. Rusanov, A. Frontera and K. V. Domasevitch, *CrystEngComm*, 2017, **19**, 1933–1937.
13 T. Basak, A. Bhattacharyya, M. Das, K. Harms, A. Bauzá, A. Frontera and S. Chattopadhyay, *ChemistrySelect*, 2017, **2**, 6286–6295.
14 A. Bhattacharyya, M. Das, A. Bauzá, S. Herrero, R. González-Prieto, A. Frontera and S. Chattopadhyay, *New J. Chem.*, 2017, **41**, 13585–13592.
15 D. Sadhukhan, M. Maiti, A. Bauzá, A. Frontera, E. Garribba and C. J. Gomez-García, *Inorg. Chim. Acta*, 2019, **484**, 95–103.
16 S. Shaygan, H. Pasdar, N. Foroughifar, M. Davallo and F. Motiee, *Appl. Sci.*, 2018, **8**, 385–397.
17 C. Verma and M. A. Quraishi, *Coord. Chem. Rev.*, 2021, **446**, 214105–214127.
18 W. Al Zoubi and Y. G. Ko, *Appl. Organomet. Chem.*, 2017, **31**, 3574–3586.
19 K. Ghosh, A. Banerjee, A. Bauzá, A. Frontera and S. Chattopadhyay, *RSC Adv.*, 2018, **8**, 28216–28237.
20 D. K. Kölmel and E. T. Kool, *Chem. Rev.*, 2017, **117**, 10358–10376.
21 D. Sadhukhan, A. Ray, G. Pilet, G. M. Rosair, E. Garribba, A. Nonat, L. J. Charbonnière and S. Mitra, *Bull. Chem. Soc. Jpn.*, 2011, **84**, 764–777.
22 D. Sadhukhan, M. Maiti, A. Bauzá, A. Frontera, E. Garribba and C. J. Gomez-García, *Inorg. Chim. Acta*, 2019, **484**, 95–103.
23 B. D. Nath, M. M. Islam, M. R. Karim, S. Rahman, M. A. A. Shaikh, P. E. Georghiou and M. Menelaou, *ChemistrySelect*, 2022, **7**, 202104290.
24 Y. Gou, J. Li, B. Fan, B. Xu, M. Zhou and F. Yang, *Eur. J. Med. Chem.*, 2017, **134**, 207–217.
25 M. A. Malik, O. A. Dar, P. Gull, M. Y. Wani and A. A. Hashmi, *MedChemComm*, 2018, **9**, 409–436.
26 M. Streater, P. D. Taylor, R. C. Hider and J. Porter, *J. Med. Chem.*, 1990, **33**, 1749–1755.
27 M. Porchia, M. Pellei, F. Del Bello and C. Santini, *Molecules*, 2020, **25**, 5814.
28 S. Adhikari, T. Bhattacharjee, R. J. Butcher, M. Porchia, M. De Franco, C. Marzano, V. Gandin and F. Tisato, *Inorg. Chim. Acta*, 2019, **498**, 119098.
29 M. V. Kirillova, A. M. Kirillov, M. F. C. G. da Silva, M. N. Kopylovich, J. J. F. da Silva and A. J. Pombeiro, *Inorg. Chim. Acta*, 2008, **361**, 1728–1737.
30 X. Luo, R. Abazari, M. Tahir, W. K. Fan, A. Kumar, T. Kalhorizadeh, A. M. Kirillov, A. R. Amani-Ghadim, J. Chen and Y. Zhou, *Coord. Chem. Rev.*, 2022, **461**, 214505.
31 J. B. Araškov, A. Višnjevac, J. Popović, V. Blagojević, H. S. Fernandes, S. F. Sousa, I. Novaković, J. M. Padrón, B. B. Holló, M. Monge and M. Rodríguez-Castillo, *CrystEngComm*, 2022, **24**, 5194–5214.
32 R. Abazari, E. Yazdani, M. Nadafan, A. M. Kirillov, J. Gao, A. M. Slawin and C. L. Carpenter-Warren, *Inorg. Chem.*, 2021, **60**, 9700–9708.
33 J. Z. Gu, Y. Cai, X. X. Liang, J. Wu, Z. F. Shi and A. M. Kirillov, *CrystEngComm*, 2018, **20**(7), 906–916.
34 G. Psomas, *Coord. Chem. Rev.*, 2020, **412**, 213259.
35 Y. Deswal, S. Asija, A. Dubey, L. Deswal, D. Kumar, D. K. Jindal and J. Devi, *J. Mol. Struct.*, 2022, **1253**, 132266.
36 K. Chkirate, K. Karrouchi, N. Dege, N. K. Sebbar, A. Ejjoummany, S. Radi, N. N. Adarsh, A. Talbaoui, M. Ferbinteanu, E. M. Essassi and Y. Garcia, *New J. Chem.*, 2020, **44**, 2210–2221.
37 A. Gaber, M. S. Refat, A. A. Belal, I. M. El-Deen, N. Hassan, R. Zakaria, M. Alhomrani, A. S. Alamri, W. F. Alsanie and E. M. Saied, *Molecules*, 2021, **26**, 2288.
38 A. Tarushi, X. Totta, A. Papadopoulos, J. Kljun, I. Turel, D. P. Kessissoglou and G. Psomas, *Eur. J. Med. Chem.*, 2014, **74**, 187–198.
39 M. Pellei, F. Del Bello, M. Porchia and C. Santini, *Coord. Chem. Rev.*, 2021, **445**, 214088.
40 B. Kaya, Z. K. Yılmaz, O. Şahin, B. Aslim and B. Ülküseven, *New J. Chem.*, 2020, **44**, 9313–9320.
41 *Bruker, SMART v5.631*, Bruker AXS Inc., Madison, WI, USA, 2001.
42 G. M. Sheldrick, *SHELXT-2014*, University of Göttingen, 2014.
43 M. J. Frisch, G. W. Trucks, H. B. Schlegel, G. E. Scuseria, M. A. Robb, J. R. Cheeseman, G. Scalmani, V. Barone, G. A. Petersson, H. Nakatsuji, X. Li, M. Caricato, A. V. Marenich, J. Bloino, B. G. Janesko, R. Gomperts, B. Mennucci, H. P.

Published on 19 December 2022. Downloaded by Jadavpur University on 5/18/2023 8:47:12 AM.

Hratchian, J. V. Ortiz, A. F. Izmaylov, J. L. Sonnenberg, D. Williams-Young, F. Ding, F. Lipparini, F. Egidi, J. Goings, B. Peng, A. Petrone, T. Henderson, D. Ranasinghe, V. G. Zakrzewski, J. Gao, N. Rega, G. Zheng, W. Liang, M. Hada, M. Ehara, K. Toyota, R. Fukuda, J. Hasegawa, M. Ishida, T. Nakajima, Y. Honda, O. Kitao, H. Nakai, T. Vreven, K. Throssell, J. A. Montgomery, Jr., J. E. Peralta, F. Ogliaro, M. J. Bearpark, J. J. Heyd, E. N. Brothers, K. N. Kudin, V. N. Staroverov, T. A. Keith, R. Kobayashi, J. Normand, K. Raghavachari, A. P. Rendell, J. C. Burant, S. S. Iyengar, J. Tomasi, M. Cossi, J. M. Millam, M. Klene, C. Adamo, R. Cammi, J. W. Ochterski, R. L. Martin, K. Morokuma, O. Farkas, J. B. Foresman and D. J. Fox, *Gaussian 16, Revision C.01*, Gaussian, Inc., Wallingford CT, 2016.

44 S. Grimme, J. Antony, S. Ehrlich and H. Krieg, *J. Chem. Phys.*, 2010, **132**, 154104.

45 F. Weigend, *Phys. Chem. Chem. Phys.*, 2006, **8**, 1057–1065.

46 S. F. Boys and F. Bernardi, *Mol. Phys.*, 1970, **19**, 553–566.

47 R. F. W. Bader, *J. Phys. Chem. A*, 1998, **102**, 7314–7323.

48 T. A. Keith, *AIMAll (Version 13.05.06)*, TK Gristmill Software, Overland Park, KS, 2013.

49 J. Contreras-García, E. R. Johnson, S. Keinan, R. Chaudret, J.-P. Piquemal, D. N. Beratan and W. Yang, *J. Chem. Theory Comput.*, 2011, **7**, 625–632.

50 E. R. Johnson, S. Keinan, P. Mori-Sánchez, J. Contreras-García, A. J. Cohen and W. Yang, *J. Am. Chem. Soc.*, 2010, **132**, 6498–6506.

51 E. A. Cobar, P. R. Horn, R. G. Bergman and M. Head-Gordon, *Phys. Chem. Chem. Phys.*, 2012, **14**, 15328–15339.

52 S. Thakur, A. Frontera and S. Chattopadhyay, *Inorg. Chim. Acta*, 2021, **515**, 120057.

53 B. Dutta, S. R. Ghosh, A. Ray, S. Jana, C. Sinha, S. Das, A. D. Jana and M. H. Mir, *New J. Chem.*, 2020, **44**(, 15857–15870.

54 B. Bagchi, *Water in Biological and Chemical Processes: From Structure and Dynamics to Function*, Cambridge University Press, Cambridge, 2013.

55 O. Fabelo, J. Pasán, L. Cañadillas-Delgado, F. S. Delgado, A. Labrador, F. Lloret, M. Julve and C. Ruiz-Pérez, *CrystEngComm*, 2008, **10**, 1743–1746.

56 D. Sun, M. Z. Xu, S. S. Liu, S. Yuan, H. F. Lu, S. Y. Feng and D. F. Sun, *Dalton Trans.*, 2013, **42**, 12324–12333.

57 S. Roy, T. Basak, S. Khan, M. G. Drew, A. Bauzá, A. Frontera and S. Chattopadhyay, *ChemistrySelect*, 2017, **2**, 9336–9343.

58 L. Yang, D. R. Powell and R. P. Houser, *Dalton Trans.*, 2007, 955–964.

59 H. Kruse, K. Mrazikova, L. d'Ascenzo, J. Sponer and P. Auffinger, *Angew. Chem.*, 2020, **132**, 16696–16703.

60 S. Li, A. Azizi, S. R. Kirk and S. Jenkins, *Int. J. Quantum Chem.*, 2020, **120**, 26361.

61 R. S. Joseyphus and M. S. Nair, *Mycobiology*, 2008, **36**, 93–98.

62 S. Mahato, N. Meheta, M. Kotakonda, M. Joshi, M. Shit, A. R. Choudhury and B. Biswas, *Polyhedron*, 2021, **194**, 114933.

63 H. Kargar, A. A. Ardakani, M. N. Tahir, M. Ashfaq and K. S. Munawar, *J. Mol. Struct.*, 2021, **1233**, 130112.

 This journal is © The Royal Society of Chemistry 2023